

# Poly(methyl methacrylate)-coated carbonyl iron particles and their magnetorheological characteristics

Wanquan Jiang,<sup>a\*</sup> Hong Zhu,<sup>a</sup> Chaoyang Guo,<sup>b</sup> Jianfeng Li,<sup>c</sup> Qun Xue,<sup>c</sup> Jianghua Feng<sup>c</sup> and Xinglong Gong<sup>b\*</sup>

## Abstract

Magnetorheological fluids (MRFs) are types of suspensions that contain magnetic particles and a carrier fluid, and are considered as semi-active smart materials. By tuning the strength of an external magnetic field, like other traditional MRFs, a carbonyl iron (CI)–poly(methyl methacrylate) (PMMA) particle-based MRF can change reversibly from a fluid-like state to a solid-like state within milliseconds. In the research reported, CI particles were encapsulated with PMMA via emulsion polymerization. After the polymerization, the fabricated CI–PMMA composite particles were dispersed in a suspension medium to prepare MRF. The synthesized CI–PMMA composite particle-based MRF showed a shear stress of 60 kPa at the magnetic field strength of 0.6 T, and a greatly enhanced anti-sedimentation stability.

© 2010 Society of Chemical Industry

**Keywords:** magnetorheological fluid (MRF); CI–PMMA composite particles; anti-sedimentation property; magnetorheological effect

## INTRODUCTION

Magnetorheological fluids (MRFs) are types of suspension that contain magnetic particles and a dispersion medium, and are considered as semi-active smart materials since they were reported in the late 1940s by Rabinow.<sup>1</sup> They exhibit the mechanical behavior of changing from a fluid-like state to a solid-like state within milliseconds with a change in the strength of an external magnetic field,<sup>2</sup> this mechanical behavior being the so-called controllable magnetorheological (MR) effect. Taking advantage of this outstanding mechanical characteristic, MRFs have been widely used in engineering applications such as dampers,<sup>3–5</sup> vibration control,<sup>6</sup> MR polishing,<sup>7</sup> MR isolators,<sup>8</sup> MRF-based haptic devices,<sup>9</sup> brakes<sup>10</sup> and so on. Since the density of most microsized magnetic particles in MRFs is markedly higher than that of the suspending medium, the magnetic particles will sediment. The problem is that this sedimentation leads to a notable decrease of the MR effect; therefore, the dispersion stability of MRFs plays a significant role in their applications and needs consideration.

Much endeavor aimed at improving the anti-sedimentation character has focused on the fabrication of magnetic particles. For instance, Cao *et al.* synthesized superparamagnetic Fe<sub>3</sub>O<sub>4</sub>/poly(methyl methacrylate) (PMMA) nanocomposites,<sup>11</sup> Li *et al.* prepared single-wall carbon nanotubes<sup>12</sup> and Kim *et al.* coated polystyrene on nanosized  $\gamma$ -Fe<sub>2</sub>O<sub>3</sub> magnetic particles.<sup>13</sup> But the magnetization saturation of these nanosized magnetic composites is too poor for engineering applications. Other similar work encapsulated carbonyl iron (CI) particles with polymer materials, like PMMA, and the composite particle-based MRFs demonstrated relatively low shear stress. Choi *et al.* prepared a composite particle-based MRF of 25 vol%, the shear stress being less than 2 kPa,<sup>14</sup> Kim *et al.* fabricated composite particles and an MRF with 25 vol% of them displayed a shear stress of

around 2 kPa,<sup>15</sup> Cho *et al.* prepared an MRF of 30 vol%, the highest shear stress being 10 kPa<sup>16</sup> and Choi *et al.* synthesized composite particles for an MRF, the shear stress of which was about 15 kPa.<sup>17</sup>

Some research has highlighted the composition of carrier fluids, which is aimed at enhancing the anti-sedimentation characteristics. For example, poly(vinyl pyrrolidone) and carbon nanotubes were added into carrier fluids as additives,<sup>18</sup> two types of CI were mixed in an ionic liquid<sup>19</sup> and polyimide gels were used as carrier media.<sup>20</sup> These methods improve the anti-sedimentation properties to some extent, but are expensive and troublesome, which limit their application in commercial fields.

In the research reported here, a PMMA layer was coated on CI particles to fabricate CI–PMMA composite particles. These composite particles were then dispersed in silicone oil to produce MRF.<sup>21</sup> This MRF shows good anti-sedimentation stability and a shear stress of about 60 kPa at the magnetic field strength of 0.6 T.

\* Correspondence to: Wanquan Jiang, Department of Chemistry, University of Science and Technology of China, Hefei, PR China. E-mail: jiangwq@ustc.edu.cn

Xinglong Gong, CAS Key Laboratory of Mechanical Behavior and Design of Materials, Department of Modern Mechanics, University of Science and Technology of China, Hefei, PR China. E-mail: gongxl@ustc.edu.cn

a CAS Key Laboratory of Mechanical Behavior and Design of Materials, Department of Modern Mechanics, University of Science and Technology of China, Hefei 230027, PR China

b Department of Chemistry, University of Science and Technology of China, Hefei 230026, PR China

c Zhuzhou Electric Locomotive Research Institute, Zhuzhou 412001, China

## EXPERIMENTAL

### Materials

Methyl methacrylate (MMA; CP), acetic acid (AR), sodium laurylsulfonate (SDS; CP), ammonium persulfate (APS; AR), sodium hydroxide (NaOH; AR), ethanol (AR) and silicone oil (H201-500) were purchased from Sinopharm Chemical Reagent Co. Ltd. CI particles (model CN) were bought from BASF, Germany, with an average diameter of 3.5  $\mu\text{m}$ .

### Preparation of CI-PMMA composite particles

The CI particles were coated with PMMA via emulsion polymerization. Before the reaction, distilled water was purified by nitrogen gas and MMA was refined by diluted NaOH solution. First, the CI particles were activated by acetic acid for a few minutes, and then washed with distilled water. Second, with a nitrogen flow to protect the iron particles from being oxidized, appropriate amounts of distilled water (500 mL), SDS (0.5 g), MMA (30 mL) and activated CI particles (100 g) were added into the system and stirred simultaneously. Next, aqueous APS solution was added dropwise to initiate the polymerization. The reaction system temperature was kept at *ca* 80 °C throughout the process. After 10 h polymerization, the black product obtained was poured out, washed with distilled water and ethanol, then separated from the by-products using magnetic power and dried in vacuum at 50 °C.

### Preparation of the MRF

Both CI particles and the composite particles were dispersed in silicone oil, separately, to prepare MRFs; the concentration of these particles was *ca* 30 vol%.<sup>22</sup>

### Characterization

The morphology of the particles was characterized using field emission SEM (JEOL, JSM-6700F) at an accelerating voltage of 5 kV. Fourier transform infrared (FTIR) spectra were acquired with a Bruker FTIR (EQUINOX55) instrument using KBr wafers. TGA was performed using a Shimadzu TGA 50 in nitrogen atmosphere, with a scanning rate of 10 °C min<sup>-1</sup> ramped from 0 to 800 °C. The samples were in alumina pans. XRD patterns were recorded using a Philips X'Pert PRD S diffractometer with monochromator for a  $2\theta$  range from 10° to 90°. X-ray photoelectron spectroscopy (XPS) was carried out using a Thermo-VG Scientific ESCALAB 250 instrument with Al K $\alpha$  radiation at a pass energy of 1486.6 eV.

The MR characterization of the MRFs was carried out at 25 °C using a rotational rheometer (Physica, MCR 301, Anton Paar, Austria) with a temperature controller. The examination was performed with a parallel-plate measuring system (PP20) with a diameter of 20 mm and a testing gap of 1 mm.<sup>23</sup>

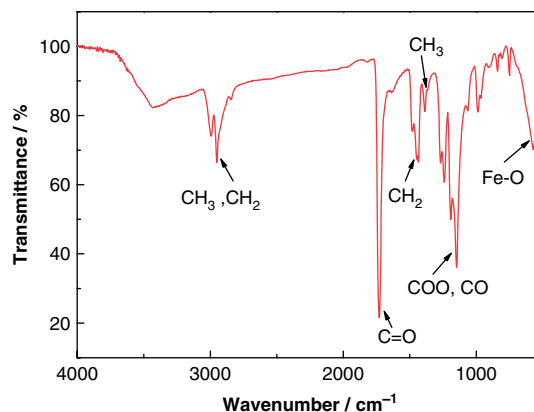


Figure 2. FTIR spectrum of CI-PMMA particles.

## RESULTS AND DISCUSSION

### Morphologies of CI-PMMA particles

SEM images of pure CI particles and CI-PMMA composite particles are shown in Fig. 1. Figure 1(b) shows an SEM image of the composite particles at a magnification of  $\times 3000$ , which indicates that all the CI particles have been encapsulated with PMMA; Fig. 1(c) shows an SEM image of a certain CI-PMMA particle at a magnification of  $\times 15\,000$ , which displays a clear morphology of the composite particle surface. The size of the CI-PMMA composite particles (4.3  $\mu\text{m}$ ) is larger than that of pure CI particles (3.5  $\mu\text{m}$ ) after the encapsulation process. Moreover, compared to pure CI particles, the surface of the composite particles is coarser and the density decreases to 5.6 g cm<sup>-3</sup>, while the density of the CI particles is 7.2 g cm<sup>-3</sup>.

### FTIR spectroscopy

The FTIR spectrum shown in Fig. 2 confirms the coating of PMMA on the surface of CI particles. The strong absorption band at 580 cm<sup>-1</sup> is assigned to the vibrations of the Fe-O group; the sharp absorption at 1730 cm<sup>-1</sup> together with the two wide absorption peaks between 1330 and 1000 cm<sup>-1</sup> indicate the presence of -CO-OR groups. Furthermore, there are no peaks in the ranges 1000-650 and 1680-1600 cm<sup>-1</sup> in relation to -C=C-, which demonstrates the completion of the polymerization process.

### Thermal stability

TGA of the CI-PMMA composite particles was conducted to evaluate the thermal stability of the particles and to estimate the approximate amount of PMMA coated on the surface of the composite particles. As shown in Fig. 3, the weight loss indicates the degradation of the coating layer. The curve in Fig. 3(a) reveals the weight loss process of the PMMA particles,<sup>17,24</sup> the temperature

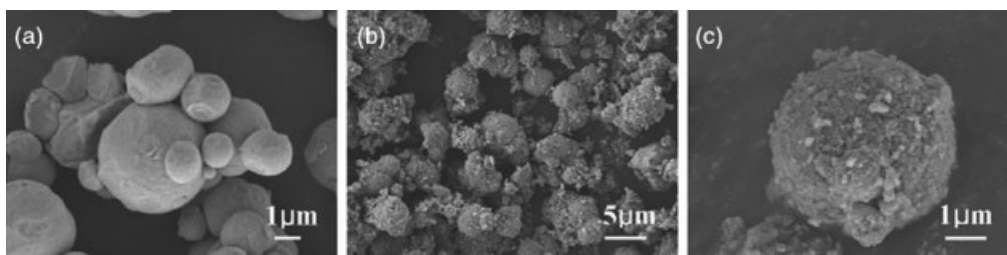
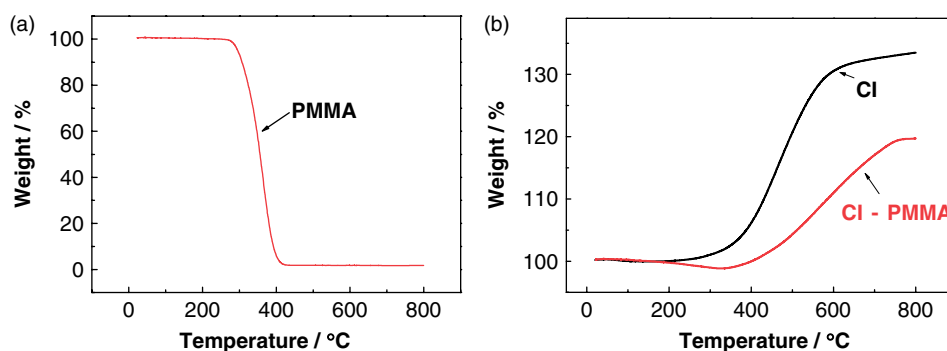


Figure 1. SEM images of (a) bare CI and (b, c) CI-PMMA particles.



**Figure 3.** TGA curves of (a) PMMA and (b) CI and CI-PMMA particles.

region of the PMMA particle degradation being 250–400 °C. In Fig. 3(b), the curves show the thermal character of the CI particles and CI-PMMA particles. A noticeable weight loss appears in the range 200–400 °C in the curve for the CI-PMMA particles, which verifies the degradation of the PMMA layer coated on the CI particles, and the content of PMMA in the CI-PMMA composite is about 5 wt%. Moreover, obvious increasing parts are observed in both curves, due to the oxidation of iron in the CI and CI-PMMA particles by the trace amount of oxygen in the nitrogen atmosphere at high temperature.

#### XPS analysis

The XPS measurements shown in Fig. 4 confirm the stable attachment of PMMA on the surface of CI particles. The quantitative results indicate that the content of iron is 31.44% and 6.2% in pure CI and CI-PMMA composite particles, respectively. Apparently, after the polymerization, the content of iron on the surface of the CI-PMMA composite particles falls dramatically, which proves the successful coating of PMMA on the surface of the CI particles. Also, the contents of carbon and oxygen for both particle types relate to the absorption of CO<sub>2</sub> on the surface. Furthermore, as for CI-PMMA particles, the PMMA layer which is made up of carbon, hydrogen and oxygen also contributes to the amount of carbon and oxygen.

#### XRD analysis

The XRD patterns of CI and CI-PMMA composite particles are shown in Fig. 5. The XRD pattern of the CI particles parallels the

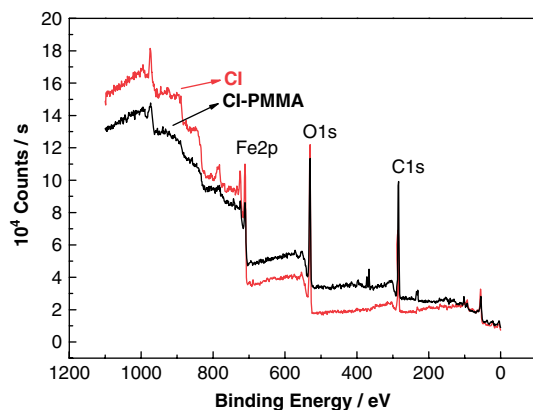


**Figure 4.** XPS spectra of CI and CI-PMMA particles.

pattern of  $\alpha$ -Fe particularly, which is verified by the standard XRD patterns with the PCPDF number of 87–0721. In this pattern, the three sharp peaks appearing at  $2\theta$  values of about 45°, 65° and 82° evidence the crystalline structure of  $\alpha$ -Fe. In the XRD pattern of the CI-PMMA particles, the three typical sharp peaks are also seen, which indicates that the polymerization procedure does not change the crystalline structure of CI.

#### MR characteristics

##### Sedimentation

In order to better observe the sedimentation characteristics, both of the MRFs, based on CI and CI-PMMA at 30 vol%, were diluted to 3 vol%.<sup>25</sup> Then, the diluted MRFs were poured into measuring cylinders (10 mL) with gum-stoppers to avoid impurity contamination. These samples were placed vertically on a static marble stage at room temperature.<sup>26,27</sup> During the process, a transparent layer forms because the magnetic particles sediment in the silicone oil.<sup>28</sup> Throughout the measurement, the volumes of the upper transparent layer were monitored over time. The formula for the sedimentation ratio ( $q$ ) is

$$q(\%) = \frac{V_0 - V_1}{V_0} \times 100$$

where  $V_0$  is the initial volume and  $V_1$  is the volume of the transparent layer.

Figure 6(a) vividly shows the sedimentation process and Fig. 6(b) shows the sedimentation ratio as a function of time. This demonstrates that the MRF with the CI-PMMA composite particles possesses longer-term stability against sedimentation in silicone oil. Figure 6(c) shows the sedimentation of MRFs of 30 vol%. The

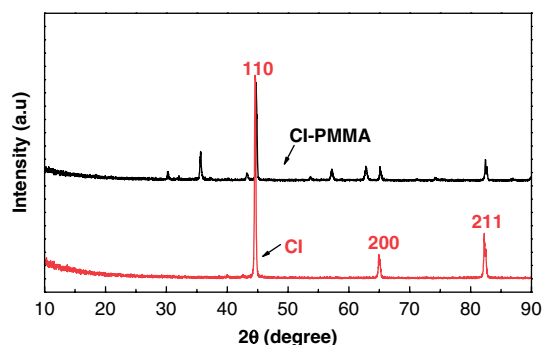


**Figure 5.** XRD patterns of CI and CI-PMMA particles.

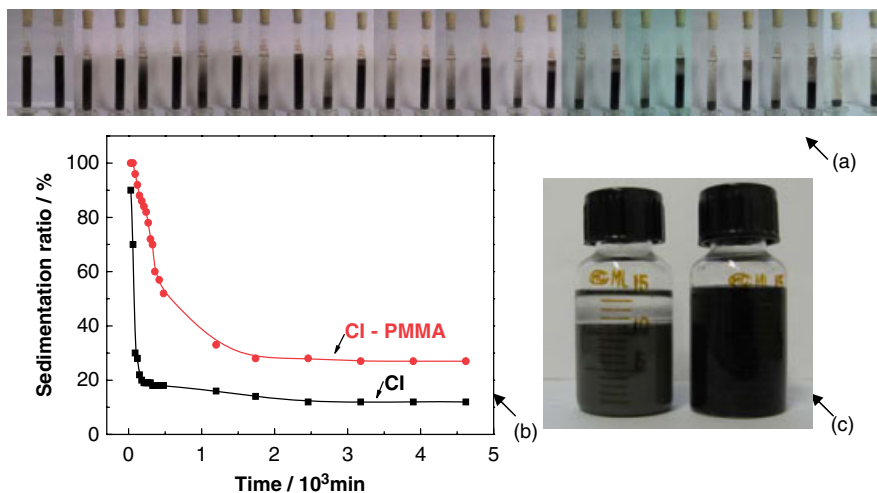


**Figure 6.** Sedimentation of CI- and CI-PMMA-based MRFs.

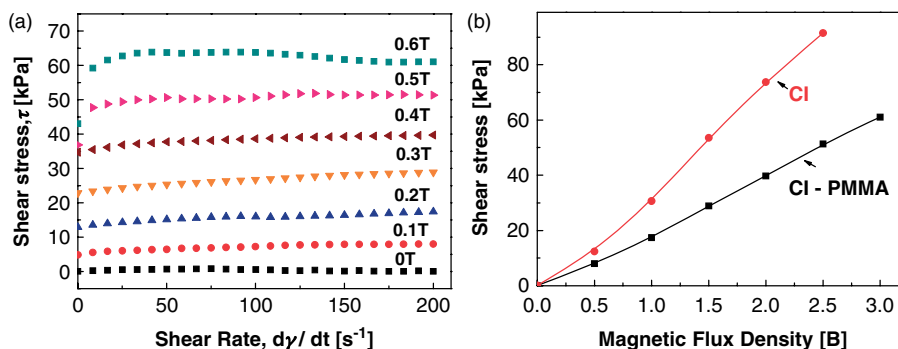


**Figure 7.** Shear stress as a function of (a) shear rate and (b) magnetic field strength.

pure CI-based MRF sediments to its equilibrium in 10 days (left), while the CI-PMMA-based MRF does not separate into two phases even over 6 months (right), which further confirms the conclusion that the CI-PMMA-based MRF exhibits a better anti-sedimentation property. Previous related work all showed anti-sedimentation character to different degrees: Chin *et al.* added Co- $\gamma$ -Fe<sub>2</sub>O<sub>3</sub> (10%) and CrO<sub>2</sub> (10%) to an MRF at a concentration of 40 vol%, which showed a sedimentation ratio of about 70%;<sup>29</sup> Fang *et al.* synthesized a polystyrene/Fe<sub>3</sub>O<sub>4</sub>-based MRF, which displayed a sedimentation ratio of 70%;<sup>30</sup> and Jang *et al.* coated CI particles with poly(vinyl butyral), and an MRF based on these composite particles showed a sedimentation of 80%.<sup>31</sup>

#### MR effect

The MR effect of the CI-PMMA-based MRF was examined as a function of external magnetic field strength controlled by current, using a rheometer with a temperature controller.<sup>32</sup> Fig. 7(a) shows shear stress as a function of shear rate at some steady magnetic flux density, and Fig. 7(b) shows shear stress as a function of magnetic flux density for a shear rate of 200  $s^{-1}$ . In both figures, the shear stress increases with increasing shear rate and magnetic field strength. The CI-PMMA-based MRF of 30 vol% displays a shear stress of about 60 kPa at a magnetic field strength of 0.6 T. This value is lower than that of the pure CI-based MRF (about 90 kPa) because of the PMMA layer, which reduces the effective content of iron in the MRF with the same volume percentage, and the polymer layer also prevents direct contact of iron encapsulated

in it. However, the shear stress of 60 kPa is still markedly higher than that found in previous similar work, for which the shear stress values are 2 kPa (25 vol%),<sup>14,15</sup> 10 kPa (30 vol%)<sup>16</sup> and 15 kPa.<sup>17</sup> In addition, the shear stress does not achieve its maximum value, as shown in Fig. 7(b), for the limits of the testing instrument, which demonstrates the potential usefulness of the CI-PMMA-based MRF.

## CONCLUSIONS

CI particles were encapsulated by crosslinked PMMA via emulsion polymerization to fabricate CI-PMMA composite particles. The CI-PMMA composite particle-based MRF showed a shear stress of 60 kPa at a magnetic strength of 0.6 T. Furthermore, the density of the CI-PMMA composite particles was less than that of pristine CI as a result of the PMMA layer. Consequently, the synthesized CI-PMMA composite particle-based MRF had dramatically improved sedimentation property and the dispersion stability in comparison to the CI-based MRF. In addition, the polymerization process is accessible and the experiment can be magnified easily, which is a requirement for potential commercial applications.

## REFERENCES

- 1 Rabinow J, *AIEE Trans* **67**:1308–1315 (1948).
- 2 Climent E, Maxey MR and Karniadakis GE, *Langmuir* **20**:507–513 (2004).

- 3 Dyke SJ, Spencer BF, Sain MK and Carlson JD, *Smart Mater Struct* **5**:565–575 (1996).
- 4 Li WH and Du H, *Int J Adv Manufact Technol* **25**:205–213 (2005).
- 5 Liu YM, Gordaninejad F, Evrensel CA, Wang XJ and Hitchcock G, *ASCE J Struct Eng* **131**:743–751 (2005).
- 6 Choi SB, Hong SR, Sung KG and Sohn JW, *Int J Mech Sci* **50**:559–568 (2008).
- 7 Kozhinova IA, Romanofsky HJ, Maltsev A, Jacobs SD, Kordonski WI and Gorodkin SR, *Appl Opt* **44**:4671–4677 (2005).
- 8 Brigley M, Choi YT, Wereley NM and Choi SB, *J Intell Mater Syst Struct* **18**:1143–1148 (2007).
- 9 Han YM, Kim CJ and Choi SB, *Smart Mater Struct* **18**:015002 (2009).
- 10 Liu B, Li WH, Kosasih PB and Zhang XZ, *Smart Mater Struct* **15**:1960–1966 (2006).
- 11 Cao Z, Jiang WQ, Ye XZ and Gong XL, *J Magn Magn Mater* **320**:1499–1502 (2008).
- 12 Li WH, Lynam C, Chen J, Liu B, Zhang XZ and Wallace GG, *Mater Lett* **61**:3116–3118 (2007).
- 13 Kim YH, Park BJ, Choi HJ and Seo Y, *Phys Stat Sol A* **204**:4178–4181 (2007).
- 14 Choi JS, Park BJ, Cho MS and Choi HJ, *J Magn Magn Mater* **304**:e374–e376 (2006).
- 15 Kim MS, Cho MS and Choi HJ, *Phys Stat Sol A* **204**:4198–4201 (2007).
- 16 Cho MS, Lim ST, Jang IB, Choi HJ and Jhon MS, *IEEE Trans Magn* **40**:3036–3038 (2004).
- 17 Choi HJ, Park BJ, Cho MS and You JL, *J Magn Magn Mater* **310**:2835–2837 (2007).
- 18 Pu HT, Jiang FJ, Yang ZL and Yan B, *J Appl Polym Sci* **102**:1653–1657 (2006).
- 19 Dobbiba G, Park HS, Okaya K and Fujita T, *J Magn Magn Mater* **320**:1322–1327 (2008).
- 20 Fuchs A, Hu B, Gordaninejad F and Evrensel C, *J Appl Polym Sci* **98**:2402–2413 (2005).
- 21 Ahmadkhanlou F, Mahboob M, Bechtel S and Washington G, *J Fluids Eng Trans ASME* **130**:121301–121307 (2008).
- 22 Dang A, Ooi L, Fales J and Stroeve P, *Ind Eng Chem Res* **39**:2269–2274 (2000).
- 23 Zubieta M, Elejabarrieta MJ and Bou-Ali M, *Rheol Acta* **48**:89–95 (2009).
- 24 Tiwari RR and Natarajan U, *Polym Int* **57**:738–743 (2008).
- 25 Guerrero-Sanchez C, Lara-Ceniceros T, Jimenez-Regalado E, Rasa M and Schubert US, *Adv Mater* **19**:1740–1747 (2007).
- 26 Lim ST, Cho MS, Jang IB and Choi HJ, *J Magn Magn Mater* **282**:170–173 (2004).
- 27 Fang C, Zhao BY, Chen L, Wu Q, Liu N and Hu KA, *Smart Mater Struct* **14**:N1–N5 (2005).
- 28 Ngatu GT and Wereley NM, *IEEE Trans Magn* **43**:2474–2476 (2007).
- 29 Chin BD, Park JH, Kwon MH and Park OO, *Rheol Acta* **40**:211–219 (2001).
- 30 Fang FF, Kim JH and Choi HJ, *Polymer* **50**:2290–2293 (2009).
- 31 Jang IB, Kim HB, Lee JY, You JL and Choi HJ, *Smart Mater Struct* **97**:10Q912 (2005).
- 32 Li WH, Chen G and Yeo SH, *Smart Mater Struct* **8**:460–468 (1999).